Int. J. Exp. Path. (2007), 88, 279–290
doi: 10.1111/j.1365-2613.2007.00540.x

ORIGINAL ARTICLE

Low coronary driving pressure early in the course of myocardial infarction is associated with subendocardial remodelling and left ventricular dysfunction

Marcia Kiyomi Koike*, Clovis De Carvalho Frimm* and Mariana Cúri†

**LIM 51 – Laboratory of Emergency Medicine, University of São Paulo Medical School and †Department of Applied Mathematics and Statistics, Institute of Mathematical and Computational Sciences of the University of São Paulo, São Carlos, SP, Brazil*

INTERNATIONAL JOURNAL OF EXPERIMENTAL PATHOLOGY

Summary

Subendocardial remodelling of the left ventricular (LV) non-infarcted myocardium has been poorly investigated. Previously, we have demonstrated that low coronary driving pressure (CDP) early postinfarction was associated with the subsequent development of remote subendocardial fibrosis. The present study aimed at examining the role of CDP in LV remodelling and function following infarction. Haemodynamics were performed in Wistar rats immediately after myocardial infarction (MI group) or sham surgery (SH group) and at days 1, 3, 7 and 28. Heart tissue sections were stained with HE, Sirius red and immunostained for α-actin. Two distinct LV regions remote to infarction were examined: subendocardium (SE) and interstitium (INT). Myocyte necrosis, leucocyte infiltration, myofibroblasts and collagen volume fraction were determined. Compared with SH, MI showed lower CDP and LV systolic and diastolic dysfunction. Necrosis was evident in SE at day 1. Inflammation and fibroplasia predominated in SE as far as day 7. Fibrosis was restricted to SE from day 3 on. Inflammation occurred in INT at days 1 and 3, but at a lower grade than in SE. CDP correlated inversely with SE necrosis ($r = -0.65$, $P = 0.003$, at day 1), inflammation ($r = -0.76$, $P < 0.001$, at day 1), fibroplasia ($r = -0.47$, $P = 0.04$, at day 7) and fibrosis ($r = -0.83$, $P < 0.001$, at day 28). Low CDP produced progressive LV expansion. Necrosis at day 1, inflammation at days 3 and 7, and fibroplasia at day 7 correlated inversely with LV function. CDP is a key factor to SE integrity and affects LV remodelling and function following infarction.

Keywords
coronary driving pressure, myocardial infarction, myocardial remodeling, subendocardial fibrosis

Received for publication:
22 November 2006
Accepted for publication:
27 April 2007

Correspondence:
Marcia K. Koike
Av. Dr. Arnaldo, 455 – sala 3134,
São Paulo, SP, Brazil
CEP 01246-903
Tel.: 55 11 3064-8756
Fax: 55 11 3061-7170
E-mail: mkoike@usp.br

Cardiac remodelling is characterized by molecular, cellular and interstitial changes of the myocardium resulting in changes in size, shape and function of the heart (Cohn *et al.* 2000). Remodelling that follows myocardial infarction manifests by wound healing at the site of wall necrosis and, depending on infarct size, by myocyte hypertrophy and

extracellular matrix changes in the remote non-infarcted myocardium, where there is evidence of excessive accumulation of collagen fibers (Volders *et al.* 1993). Interstitial fibrosis is recognized as a key pathological change of remodelling and to predispose the heart to cardiac dysfunction (Wilke *et al.* 1996; Van Kerckhoven *et al.* 2000). The pathological changes that occur in the non-infarcted subendocardial region have been poorly investigated so far (Michel *et al.* 1988). In fact, subendocardial accumulation of fibrosis in the remote myocardium does occur and seems to be accounted for the impairment of the coronary perfusion pressure early in the course of infarction (de Carvalho Frimm *et al.* 2003). In infarcts of large magnitude, the haemodynamic changes that follow coronary artery occlusion, particularly the increase in left ventricular end-diastolic pressure concurrent with the decrease in systemic blood pressure, contribute to the impairment of coronary perfusion and may thus jeopardize the integrity of the non-infarcted myocardium. As the subendocardium is the myocardial layer most likely affected by perfusion deficits (Toyota *et al.* 2005), it is reasonable to suppose that in some yet unrecognized extent prolonged subendocardial ischaemia would further affect ventricular remodelling. In that case, subendocardial fibrosis may indeed represent a reparative process contrasting to reactive interstitial fibrosis that appears in the remainder layers of the non-infarcted myocardium (Weber *et al.* 1989). By interfering with myocardial integrity, subendocardial injury may therefore be implicated in postinfarction ventricular dysfunction.

The main objectives of the present study were twofold: (i) to investigate the role of coronary driving pressure in subendocardial remodeling, and (ii) to evaluate the role of subendocardial pathological changes in left ventricular function, using a rat model of myocardial infarction. Of particular additional interest was the evaluation of left ventricular remodelling, taking into account two distinct layers of the remote non-infarcted regions: the subendocardium and the interstitial space corresponding to the remainder myocardial layers.

Materials and methods

All procedures were carried out in accordance with the norms of the Brazilian College of Animal Research and The Universities Federation for Animal Welfare. Our Institutional Ethical Committee approved the protocol.

Male Wistar rats weighing 300–350 g were used. Four groups of rats with myocardial infarction (MI) and their respective sham controls (SH) were constituted according to the interval of follow-up: (i) early acute phase: MI 1 (n = 9) and SH 1 (n = 9), 1 day; (ii) late acute phase: MI 3 (n = 15) and SH 3 (n = 16), 3 days; (iii) subacute phase: MI 7 (n = 9) and SH 7 (n = 10), 7 days; and (iv) chronic phase: MI 28 (n = 11) and SH 28 (n = 11), 28 days.

Haemodynamic measurements

Initial and final haemodynamic measurements were determined after the experimental surgery and at the end of the follow-up respectively. Animals were anaesthetized with intraperitoneal Ketamine, 50 mg/kg, and Pentobarbital, 25 mg/kg. Systemic and left ventricular blood pressures were determined simultaneously via femoral and carotid catheters introduced into the abdominal aorta and into the left ventricular cavity respectively. The animals were put under mechanical ventilation (Model 683; Harvard Apparatus Inc., South Natick, MA, USA) and submitted to left coronary artery ligation or sham operation, according to a previously described technique (Selye *et al.* 1960). Haemodynamics were continuously recorded during 30 min after the closure of the chest wall. The average of each beat-to-beat measurement registered during the last 10 min was considered for analysis.

The following parameters were computed: mean arterial blood pressure (mmHg), left ventricular end-diastolic pressure (mmHg), left ventricular systolic pressure (mmHg), maximum rate of increase of left ventricular pressure (+dP/dt, mmHg/s), and maximum rate of decrease of left ventricular pressure (−dP/dt, mmHg/s). The last two were used to estimate left ventricular systolic and diastolic function respectively.

Coronary driving pressure (mmHg) was calculated as the difference between mean arterial blood pressure and left ventricular end-diastolic pressure. It was used to estimate the pressure gradient for left ventricular blood flow (Cross *et al.* 1961).

At the end of each follow-up period (days 1, 3, 7 and 28), haemodynamics were repeated under the same conditions.

Heart morphometric study

After euthanasia with overdose anaesthesia and cadmium chloride administration, the heart was preserved by retrograde perfusion-fixation with 10% formalin in a phosphate-buffered saline solution. The perfusion pressure employed corresponded to the *in vivo* systemic diastolic blood pressure. The heart was then removed, the atria were trimmed away, and the ventricular weight index (mg/g) was calculated by normalizing ventricular weight to body weight. After fixation, a 1–2 mm coronal slice of the heart, including both ventricles at the equatorial plane, was embedded in paraffin and cut into 5 μm sections. Tissue sections were stained with haematoxylin–eosin (HE), Sirius red, alcian blue pH 2.5,

and also underwent immunohistochemistry. A digital image analysis system (Leica Imaging Systems Ltd., Cambridge, UK) was used for morphometric measurements.

The ratio between endocardial infarct surface length and total left ventricular endocardial circumference and the ratio between epicardial infarct surface length and total left ventricular epicardial circumference were averaged to calculate infarct size (Pfeffer *et al.* 1985).

Left ventricular expansion index was calculated according to the following formula:

Left ventricular expansion index = (left ventricular cavity area/left ventricular total area) x (interventricular septum thickness/infarct wall thickness) (Whittaker *et al.* 1991).

The same formula was used to calculate left ventricular expansion index in sham animals, replacing the infarct wall thickness by the left ventricular free wall thickness.

Remote non-infarcted myocardium

Two regions were analysed separately – the subendocardium and the interstitium. The subendocardium was defined as corresponding to the inner third of the non-infarcted left ventricular region and the interstitium as the remainder outer two-thirds.

The amount of pathological changes in the subendocardium was estimated by the subendocardial lesion area (SE lesion, %) in HE-stained sections. It was calculated as the per cent ratio between the area of the subendocardium affected by inflammatory cell and/or collagen infiltration and the entire area of the remote non-infarcted left ventricular wall.

To estimate cardiomyocyte hypertrophy, HE-stained sections were examined under ×1000 magnification. The myocyte diameter (μm) around oval and central nuclei of longitudinally displayed myocytes was measured.

For each of the following measurements, the entire subendocardial region and a total of 20 interstitial microscopic fields were examined.

Myocyte necrosis (cells/mm^2) was estimated in HE-stained sections under ×1000 magnification. Nuclear pyknosis and karyolysis as well as cytoplasmic changes including vacuolization, contraction bands and hypereosinophilia were taken into account altogether (Kumar *et al.* 2004).

Leucocyte cell infiltration (cells/mm^2) was estimated in HE-stained sections under ×1000 magnification. Inflammatory cells were identified by nuclear and cytoplasmic morphological aspects. Cells with morphological characteristics of fibroblasts, cardiomyocytes, endothelial vascular cells and smooth muscle vascular cells were excluded.

Glycosaminoglycan fraction (%) was estimated in alcian blue-stained sections under ×1000 magnification. The main non-sulphated glycosaminoglycan identified by this method is hyaluronic acid (Baldwin *et al.* 1994). Glycosaminoglycan fraction was determined as the percentage of cyan blue-stained areas per total myocardial area, excluding perivascular regions.

Fibroplasia was estimated by measuring positive α-smooth muscle actin myofibroblasts (cells/mm^2) detected by immunohistochemistry under ×1000 magnification. The tissue sections were incubated overnight with a 1:500 dilution of the mouse anti-human α- smooth muscle actin antibody (Sigma Chemical Co, St Louis, MO, USA) at 4 °C. Sections were then incubated with labelled streptavidin-biotin peroxidase kit (Dako LSAB+ kit; Dako Corporation, Carpinteria, CA, USA) and diaminobenzidine for colour development. Finally, the sections were faintly counterstained with haematoxylin. Vascular smooth muscle cells with intense staining were used as positive controls. Negative controls were obtained by omitting the primary antibody and using a non-immune bovine serum.

Collagen volume fraction (%) was estimated in Sirius red-stained sections under ×580 magnification. Collagen volume fraction was determined as the percentage of red-stained connective tissue areas per total myocardial area, excluding perivascular areas.

Statistical analysis

Data are expressed as mean ± SEM. One-way analysis of variance and one-way repeated measures analysis of variance complemented by the Wald test were used to compare the groups. The hypothesis of interaction between MI and SH groups and among the different intervals of follow-up was tested beforehand.

Linear regression was used to test the following potential relationships: (i) initial coronary driving pressure and left ventricular dilatation; (ii) initial coronary driving pressure and morphometric variables in remote non-infarcted myocardium; and (iii) morphometric variables and left ventricular function at the end of each follow-up. Normality and equal variance were tested in all analyses. Statistical significance was established at $P < 0.05$. All analyses were performed using SAS software (Statistical Analysis System, version 9.1; SAS Institute Inc., Cary, NC, USA).

Results

Haemodynamic variables

The initial haemodynamic parameters measured immediately after the experimental procedure and the final values obtained at the end of each follow-up period are depicted in Table 1.

Table 1 Initial haemodynamic variables determined immediately after surgery and final haemodynamic variables determined at the end of 1, 3, 7, and 28 days of follow-up

Groups (*n*)	SH 1 (9)	MI 1 (9)	SH 3 (16)	MI 3 (15)	SH 7 (10)	MI 7 (9)	SH 28 (11)	MI 28 (11)
MAP (mmHg)								
Initial	114 ± 4	85 ± 6*	107 ± 3	95 ± 6*	100 ± 6	85 ± 6*	108 ± 3	93 ± 5*
Final	111 ± 5	86 ± 6*	101 ± 4	86 ± 5*	101 ± 4	79 ± 8*	97 ± 9	94 ± 4*
LVSP (mmHg)								
Initial	132 ± 5	104 ± 6*	126 ± 4	117 ± 6*	123 ± 5	103 ± 6*	127 ± 5	112 ± 5*
Final	133 ± 7	107 ± 6*	125 ± 5	113 ± 5*	128 ± 4	105 ± 8*	127 ± 9	112 ± 4*
LVEDP (mmHg)								
Initial	5.0 ± 0.8	12.6 ± 1.3*	5.4 ± 0.5	11.2 ± 1.3*	5.5 ± 0.7	10.1 ± 1.4*	5.5 ± 0.4	10.2 ± 1.2*
Final	5.3 ± 0.8	10.6 ± 1.0*	4.9 ± 0.5	9.1 ± 1.5*	6.0 ± 0.8	13.7 ± 3.4*	7.3 ± 0.5	10.6 ± 2.1*
CDP (mmHg)								
Initial	109 ± 4	72 ± 7*	102 ± 4	83 ± 7*	95 ± 6	75 ± 7*	102 ± 3	83 ± 6*
Final	106 ± 4	75 ± 5*	96 ± 4	78 ± 4*	95 ± 4	65 ± 9*	90 ± 9	84 ± 5*
+dP/dt (mmHg/s)								
Initial	8310 ± 570	5728 ± 336*	7757 ± 411	6557 ± 518*	7451 ± 718	5374 ± 376*	8045 ± 448	6099 ± 406*
Final	7730 ± 602	5907 ± 382*	7432 ± 384	6673 ± 410*	7574 ± 305	4973 ± 639*	7002 ± 665	6065 ± 310*
−dP/dt (mmHg/s)								
Initial	6648 ± 505	3248 ± 300*	6269 ± 405	4112 ± 373*	5446 ± 518	3316 ± 289*	6113 ± 364	3822 ± 384*
Final	6840 ± 376	4858 ± 303*†	6524 ± 259	4775 ± 264*	6750 ± 665	4045 ± 555*†	6057 ± 818	5184 ± 512†

SH, sham group; MI, myocardial infarction group; MAP, mean arterial pressure; LVSP, left ventricular systolic pressure; LVEDP, left ventricular end-diastolic pressure; CDP, coronary driving pressure; +dP/dt, maximum positive first derivative of left ventricular pressure; −dP/dt, maximum negative first derivative of left ventricular pressure.
*$P < 0.05$ *vs.* SH.
†$P < 0.05$ final *vs.* initial.

The mean arterial pressure was lower in all MI groups compared with SH, both initially and at the end of each follow-up. In each MI group, the final mean arterial pressure did not change from initial values and there was no significant difference of mean arterial pressure among the four succeeding follow-up periods. Correspondingly, left ventricular systolic pressure was also lower in all MI groups compared with SH. In each MI group, the initial and final left ventricular systolic pressure did not differ and there was no significant change among the succeeding follow-up periods.

Left ventricular end-diastolic pressure was 1.5- to 2.5-fold greater in MI groups compared with SH, both immediately after infarction and at the end of follow-up. In each MI group, final left ventricular end-diastolic pressure did not change from initial values and there was no significant difference of left ventricular end-diastolic pressure among the four succeeding follow-up intervals. Accordingly, coronary

Table 2 Morphometric parameters of left ventricular remodelling investigated at the end of each of the four periods of follow-up: 1, 3, 7, and 28 days

Groups	SH 1	MI 1	SH 3	MI 3	SH 7	MI 7	SH 28	MI 28
IS (%)		40 ± 4		37 ± 3		37 ± 5		39 ± 5
LVEI	0.22 ± 0.03	0.47 ± 0.08*	0.25 ± 0.03	0.64 ± 0.06*	0.26 ± 0.04	1.32 ± 0.27*††	0.25 ± 0.04	1.44 ± 0.38*
SE lesion (%)	0.35 ± 0.25	8.08 ± 3.36*	0.24 ± 0.15	7.04 ± 2.71*	0.32 ± 0.32	2.82 ± 1.37*††	0.52 ± 0.26	0.63 ± 0.21*†††
VW (mg/g)	5.45 ± 0.23	4.89 ± 0.22	4.69 ± 0.26	3.65 ± 0.30	3.74 ± 0.12	4.00 ± 0.09	3.68 ± 0.13	3.84 ± 0.18
Myocyte Ø (μm)	10.69 ± 0.09	11.25 ± 0.26*	9.70 ± 0.31	10.28 ± 0.38*†	9.88 ± 0.19	11.67 ± 0.48*††	9.56 ± 0.21	11.02 ± 0.41*
Body weight (g)	302 ± 3	301 ± 4	300 ± 3	302 ± 5	322 ± 5	310 ± 3	376 ± 6	380 ± 11

SH, sham group; MI, myocardial infarction group; IS, infarct size; LVEI, left ventricular expansion index; VW, ventricular weight; Ø, diameter; SE, subendocardial.
*$P < 0.05$ *vs.* SH.
†$P < 0.05$ *vs.* MI 1; ††$P < 0.05$ *vs.* MI 3; †††$P < 0.05$ *vs.* MI 7.

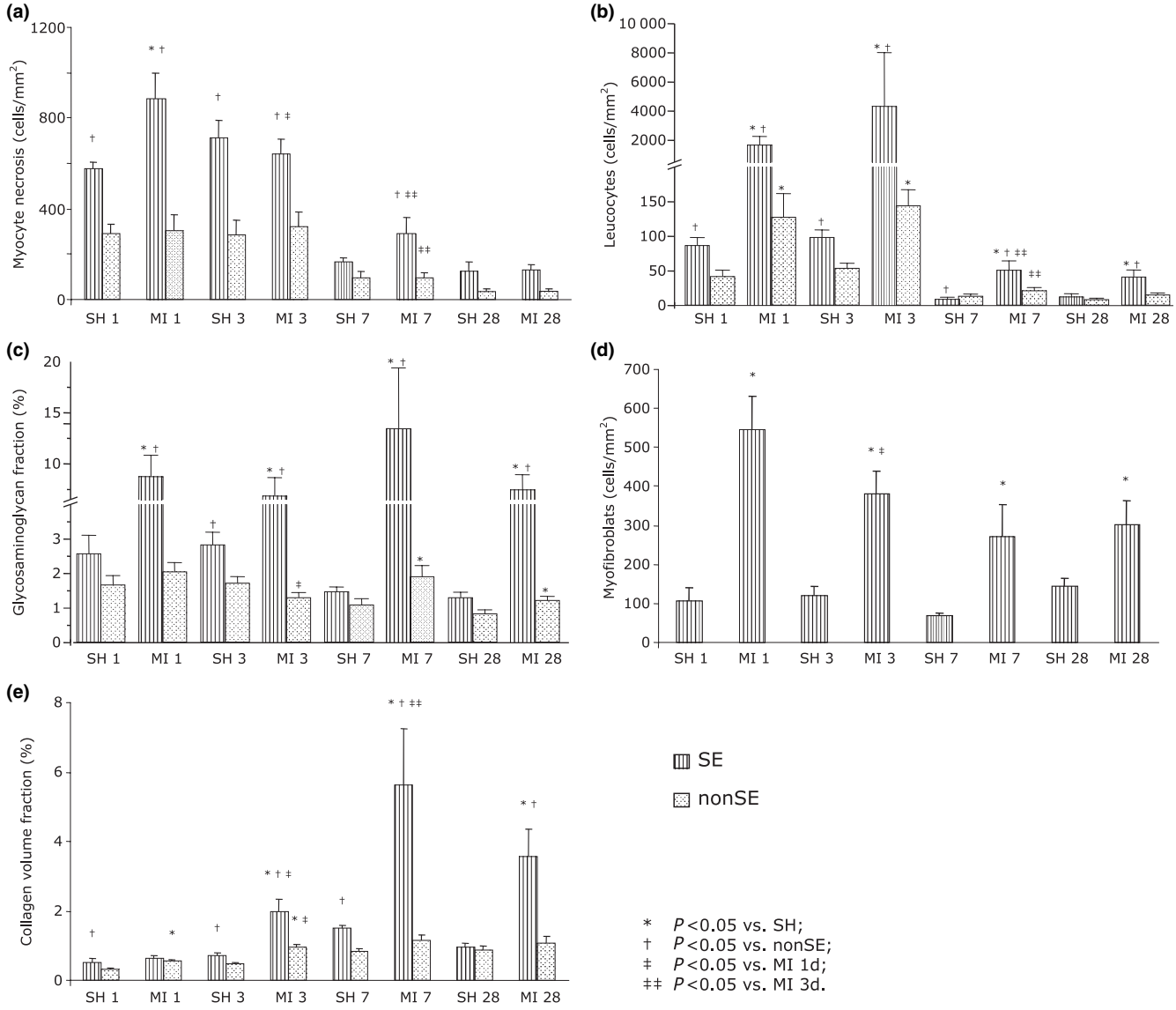

Figure 1 Pathological changes examined in two distinct non-infarcted myocardial regions, subendocardium and interstitium, at the end of 1, 3, 7 and 28 days of follow-up: (a), myocyte necrosis; (b), inflammation; (c), glycosaminoglycans; (d), fibroplasia and (e), fibrosis.

driving pressure followed the pattern observed for systemic blood pressure and left ventricular end-diastolic pressure. In average, it was 22% lower in MI groups compared with SH. Final and initial values did not differ and there was no significant difference of coronary driving pressure among the four succeeding follow-up intervals.

MI groups had +dP/dt 13% to 31% lower than that of SH. In each MI group, final +dP/dt did not differ from initial values and there was no significant difference of +dP/dt among the four succeeding follow-up intervals. As for −dP/dt, it was lower in all MI groups than SH except for final −dP/dt in MI 28. Final −dP/dt in this group (and also in MI 1 and MI 7) was higher than values taken immediately after infarction.

Morphometry

Left ventricular remodelling. Parameters of left ventricular remodelling are depicted in Table 2. Infarct size was comparable among all MI groups regardless of the period of follow-up. A twofold increase in left ventricular chamber size occurred as early as day 1 after infarction. Maximal left ventricular

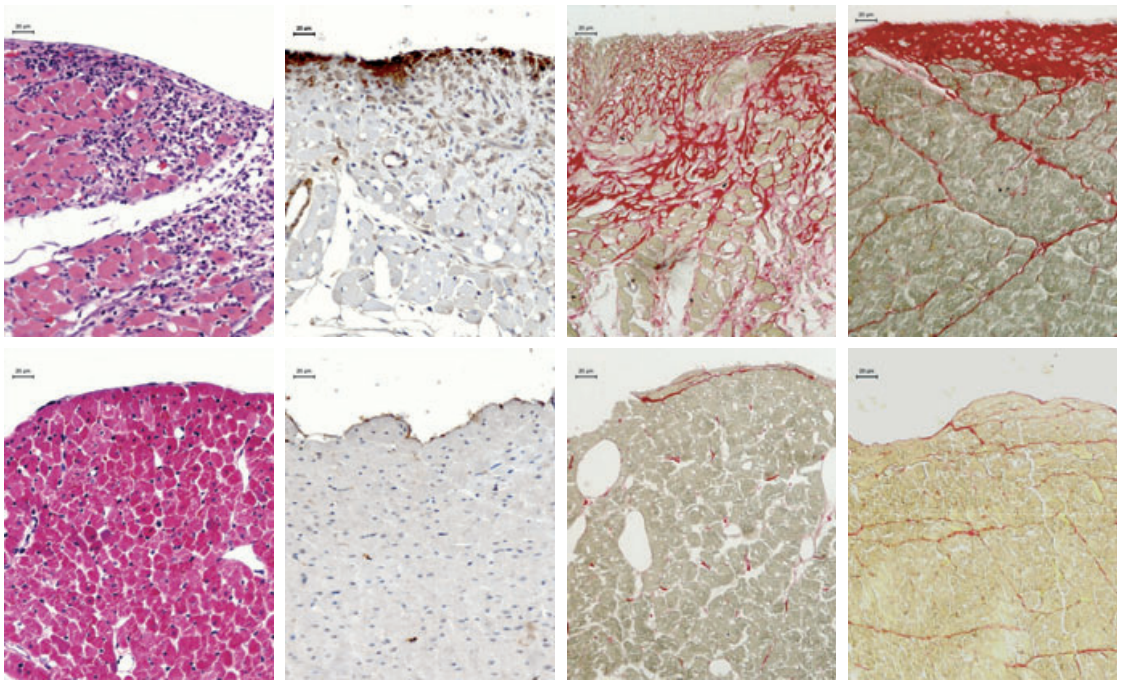

Figure 2 Photomicrographs depicting non-infarcted subendocardial regions of the left ventricle in the rat model of infarction. Top panels represent rats with myocardial infarction and bottom panels sham animals. Left panels show inflammatory cell reaction in HE-stained tissue sections at day 3. Left middle panels show myofibroblasts positive to α-smooth muscle actin immunostaining (brown cytoplasm) in tissue sections co-stained with haematoxylin at day 7. The last two right panels show red stained fibrosis in Sirius red-stained tissue sections at days 7 and 28 respectively. Prominent differences in each of these phases of subendocardial remodelling of the non-infarcted left ventricular myocardium can be observed between infarcted and sham rats.

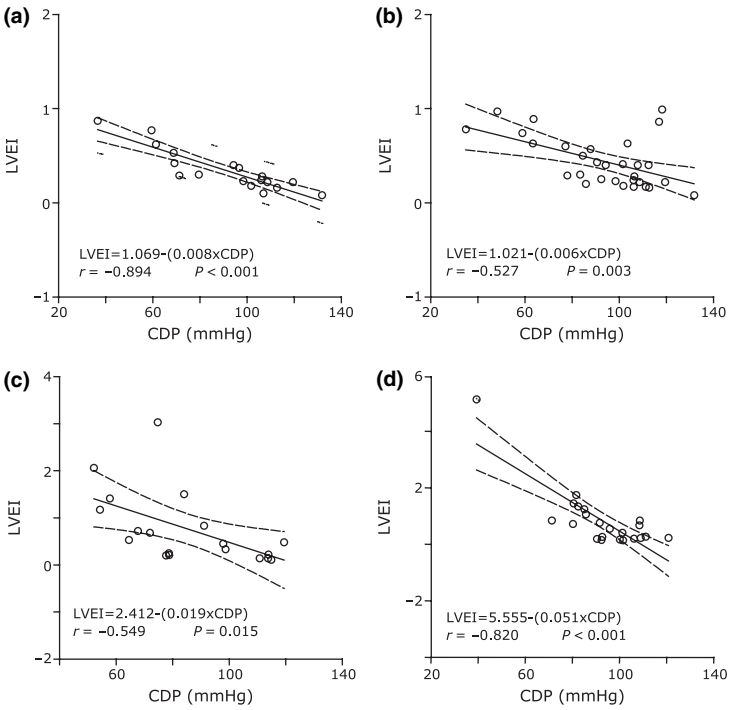

Figure 3 Relationships found between initial coronary driving pressure (CDP) and subsequent left ventricular expansion index (LVEI) measured at days 1 (panel A), 3 (panel B), 7 (panel C), and 28 (panel D). Lower initial CDP values were associated with larger left ventricular dimensions at each time point investigated.

Table 3 Relationships between initial coronary driving pressure and the different types of subendocardial lesions in the remote non-infarcted myocardium investigated at the end of each of the four periods of follow-up. Only correlation coefficients with statistical significance are represented

	day 1	day 3	day 7	day 28
Initial coronary driving pressure *vs.* left ventricular subendocardial remodelling				
Myocyte necrosis	−0.65	ns	ns	ns
Leucocyte infiltration	−0.76	−0.44	−0.53	ns
Glycosaminoglycan fraction	−0.65	ns	ns	−0.58
Fibroplasia	−0.67	−0.38	−0.47	−0.46
Collagen volume fraction	ns	ns	−0.50	−0.83

ns, non-significant; $P > 0.05$.

expansion occurred in MI rats at day 7, when left ventricular expansion index was fivefold greater than that of SH rats.

The subendocardial area of the remote non-infarcted left ventricular wall with pathological changes was largest at day 1 and then decreased progressively up to day 28. This result corresponds to a predominant cellular infiltration occupying a relatively larger endocardial region in the early phases postinfarction in contrast to a predominant fibrosis deposition occupying a relatively thinner endocardial region at the chronic phase.

Ventricular weight did not differ between MI and SH groups at any time point studied. Myocyte hypertrophy was already evident in the remote non-infarcted myocardium at day 1, was maximal at day 7 and then remained unchanged.

Remote non-infarcted myocardium. The main pathological changes that were investigated to distinguish the remodelling of the subendocardial region from that observed in the interstitium of the remainder layers of the non-infarcted left ventricle are represented in Figure 1.

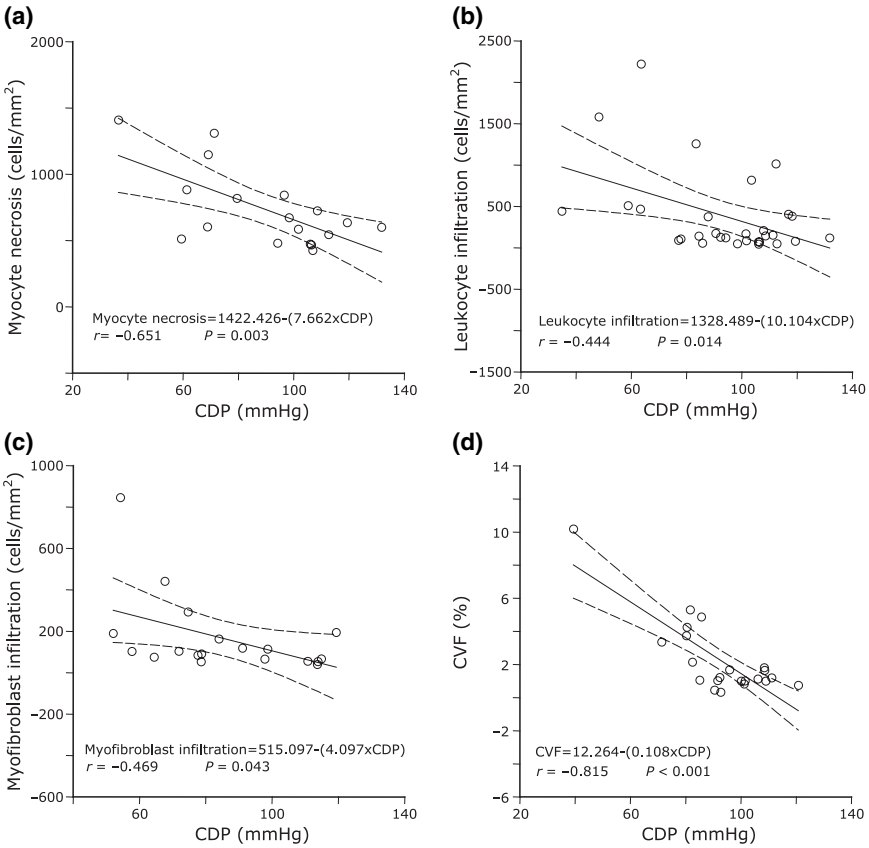

Figure 4 Relationships found between initial coronary driving pressure (CDP) and subsequent subendocardial lesions representative of myocyte necrosis at day 1 (panel A), leukocyte infiltration at day 3 (panel B), myofibroblast infiltration at day 7 (panel C), and fibrosis estimated by collagen volume fraction (CVF, panel D) at day 28.

Table 4 Relationships between the different types of left ventricular subendocardial lesions in the remote non-infarcted myocardium and left ventricular systolic and diastolic function at the end of each of the four periods of follow-up. Only correlation coefficients with statistical significance are represented

	+dP/dt				−dP/dt			
	day 1	day 3	day 7	day 28	day 1	day 3	day 7	day 28
Myocyte necrosis	ns	ns	ns	ns	−0.53	ns	ns	ns
Leucocyte infiltration	ns	−0.51	−0.52	ns	ns	−0.65	−0.46	ns
Glycosaminoglycan fraction	ns	ns	−0.63	ns	−0.48	ns	−0.54	ns
Fibroplasia	ns	ns	−0.55	ns	−0.61	−0.72	−0.55	ns
Collagen volume fraction	ns	ns	−0.55	ns	ns	−0.50	−0.47	ns

+dP/dt, maximum positive first derivative of left ventricular pressure; −dP/dt, maximum negative first derivative of left ventricular pressure; ns, non-significant; $P > 0.05$.

Myocyte necrosis was evident in the subendocardial region and was of greater magnitude in MI rats than in SH at day 1. Subendocardial myocyte necrosis decreased progressively up to day 7 in MI rats.

Leucocyte infiltration was greater in the subendocardial region of MI rats compared with SH at days 1, 3, 7 and 28. In the interstitium, leucocyte infiltration was much less evident but still more pronounced in MI rats than in SH at days 1 and 3. In MI rats, leucocyte infiltration within the subendocardium was maximal at days 1 and 3, decreased at day 7, and then remained unchanged. Similarly, in the interstitium, leucocyte infiltration was maximal at days 1 and 3, decreased at day 7, and then remained unchanged.

The increase in glycosaminoglycan fraction was again predominant in the subendocardial region, being greater in MI rats compared with SH regardless the follow-up intervals. The increase in subendocardial glycosaminoglycan fraction

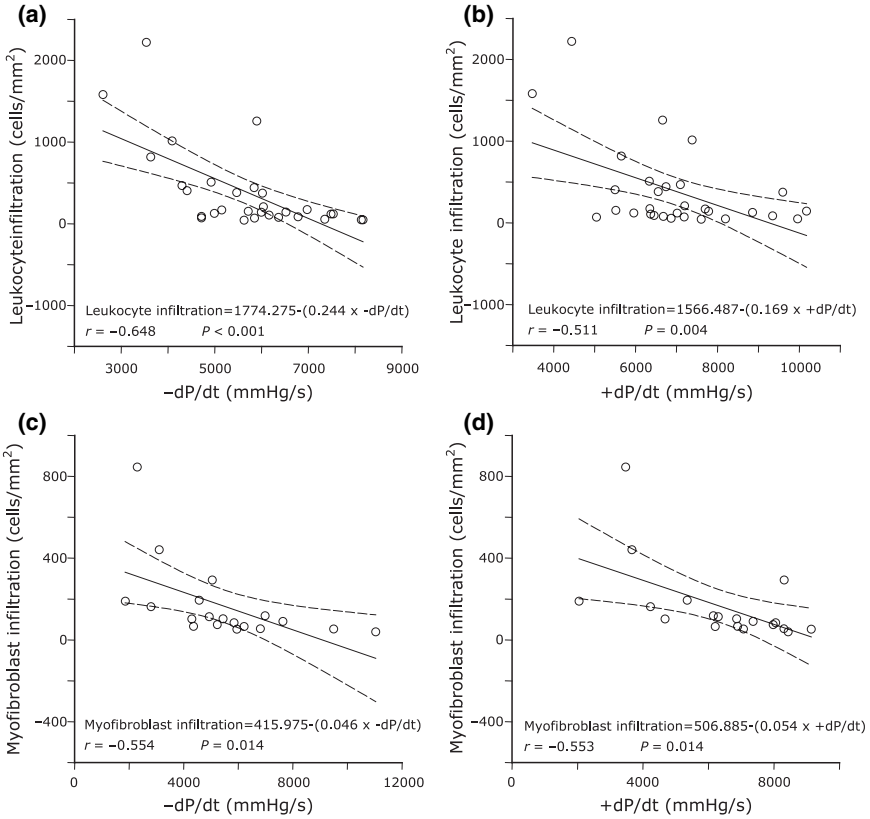

Figure 5 Relationships found between subendocardial lesions and left ventricular systolic function (+dP/dt) and diastolic function (−dP/dt). In panels A and B, the inverse correlations found between leucocyte infiltration and left ventricular function at day 3 are represented. In panels C and D, the inverse correlations between myofibroblast infiltration and left ventricular function at day 7 are represented.

remained constant up to day 28. In the left ventricular interstitium, the glycosaminoglycan fraction of MI rats was greater than in SH at days 7 and 28.

Myofibroblasts were found almost exclusively in the subendocardium, where in MI rats they outnumbered SH by 3- to 5-fold regardless the follow-up interval. The highest numbers were observed at day 1, fell by 30% at day 3, and thereafter remained statistically unchanged.

The increase in collagen volume fraction observed in MI rats as compared with SH was again predominant in the subendocardial region and observed from day 3 on. In the interstitium, fibrosis deposition was much less evident. Moreover, interstitial collagen did not differ substantially between MI and SH groups.

In Figure 2 are depicted the different phases of subendocardial remodelling.

Relationship between initial coronary driving pressure and left ventricular remodelling. There were inverse correlations between the initial coronary driving pressure and the left ventricular expansion index at all follow-up intervals investigated: day 1, day 3, day 7, and day 28 (Figure 3).

Relationship between initial coronary driving pressure and remote non-infarcted myocardium. Initial coronary driving pressure was inversely related to different left ventricular subendocardial lesions according to the time point when each of these lesions was more pronounced. These results are represented in Table 3 and in Figure 4. Low coronary driving pressure was associated with more intense myocyte necrosis at day 1, with leucocyte cell infiltration during the first 7 days, and with fibrosis at days 7 and 28. While coronary driving pressure was inversely related to glycosaminoglycans at early and late phases of infarction, the association with fibroplasia was apparent during all time points investigated.

Initial coronary driving pressure was weakly correlated with interstitial leucocyte infiltration only at the late acute phase and with glycosaminoglycans and collagen only at the subacute and chronic phases.

Relationship between remote non-infarcted myocardium and left ventricular function. The following left ventricular subendocardial lesions were inversely associated with systolic function, assessed by +dP/dt: leucocyte cell infiltration at days 3 and 7, and glycosaminoglycan fraction, fibroplasia, and collagen volume fraction at day 7.

The following left ventricular subendocardial lesions were inversely associated with diastolic function, assessed by −dP/dt: myocyte necrosis at day 1, leucocyte cell infiltration at days 3 and 7, glycosaminoglycan fraction at days 1 and 7, fibroplasia at days 1, 3, and 7, and collagen volume fraction at days 3 and 7.

Interstitial collagen volume fraction was not related to either +dP/dt or −dP/dt at any of the follow-up intervals studied. In contrast, interstitial glycosaminoglycan fraction did relate to −dP/dt at day 7 ($r = -0.63$; $P = 0.004$) and to +dP/dt at days 7 ($r = -0.47$; $P = 0.04$) and 28 ($r = -0.51$; $P = 0.03$) (Table 4 and Figure 5).

Discussion

The present study demonstrated that coronary driving pressure lowers immediately after infarction and remains low for at least 28 days. The pathological changes in the remote non-infarcted regions were represented by myocyte necrosis, inflammatory cell infiltration, increased glycosaminoglycans, fibroplasia and fibrosis accumulation, all of them predominating in the subendocardial layer of the left ventricle. The decrease in coronary driving pressure was associated with the appearance of each of these different subendocardial lesions, according to the period when they were more pronounced. Moreover, low perfusion pressure was inversely related to the progressive dilatation of the left ventricle. Subendocardial changes implicated in left ventricular diastolic and systolic dysfunction at the acute and subacute phases post infarction. These findings corroborate the speculation that subendocardial damage occurs by an ischaemia-related mechanism and is followed by progressive left ventricular remodelling.

The prevailing haemodynamic changes observed at different intervals in this study characterize large magnitude infarctions often resulting in ventricular remodelling and dysfunction (Pfeffer *et al.* 1979). The average infarct size was 35% in all groups. In MI rats, ventricular weight was comparable with that of SH documenting, in view of myocyte enlargement, the development of hypertrophy of the remote non-infarcted myocardium. The appearance of left ventricular systolic dysfunction in large infarcts may seemingly play a pivotal role in further impairing coronary perfusion pressure as far as systemic blood pressure decreases and left ventricular filling pressure raises. Accordingly, a vicious haemodynamic cycle characterized by poor left ventricular function, low perfusion pressure and subendocardial injury is established immediately after infarction and gives rise to progressive cardiac chamber dilatation. In this circumstance, coronary driving pressure becomes critical, especially if we take into account that coronary flow reserve may be also impaired (Karam *et al.* 1990).

The observation of coagulation necrosis of myocytes, leucocyte cell infiltration, fibroplasia and fibrosis corroborates the assumption of ongoing ischaemia followed by a reparative

process of wound healing taking place in the remote subendocardium. This region is reported as the myocardial layer most susceptible to underperfusion states (Toyota *et al.* 2005; Wang *et al.* 2005). Inflammation, although much more marked at the acute phases, was still present at the chronic phase when coronary driving pressure remained low. The relationship found between low coronary driving pressure and subendocardial damage at different intervals postinfarction suggests a key role for persistent subendocardial ischaemia in cardiac remodeling. Acute and subacute subendocardial changes, but not subendocardial fibrosis at day 28, explained left ventricular dysfunction. As the area of subendocardial lesion was larger at the early phases, when the granulation tissue predominated, than that found at the chronic phase, when fibrosis predominated, it is likely that the former better represents the amount of myocardial tissue damage in that region. In fact, as remodelling progresses subendocardial scar thinning develops. The abundant subendocardial changes implicated in acute and subacute left ventricular dysfunction were no more apparent at the chronic phase.

In addition to the large amounts of glycosaminoglycans identified by alcian blue staining in the subendocardial region, increased glycosaminoglycan fraction was also found in the interstitium. Interestingly, interstitial glycosaminoglycan fraction showed an inverse relationship with left ventricular function at subacute and chronic phases, probably pointing out to a role for extracellular matrix remodelling of the interstitium in sustaining cardiac dysfunction. The main non-sulphated glycosaminoglycan present in the extracellular matrix is hyaluronic acid. Hyaluronic acid plays a role in inflammatory processes by promoting interstitial oedema (Waldenstrom *et al.* 1991) and facilitating the migration and proliferation of macrophages (Savani *et al.* 2000). Recently, a hyaluronic acid-rich provisional matrix has been demonstrated to antedate fibrosis during infarct wound healing (Dobaczewski *et al.* 2006).

In contrast to many previous studies (Sun *et al.* 2000; Wei *et al.* 2000; Yu *et al.* 2001), there was no evidence of increased fibrillar collagen in the interstitium where myofibroblasts were likewise scarcely found. It is likely that a number of previous investigations by not examining separately subendocardial and interstitial regions have thus overestimated interstitial fibrosis. On the other hand, it is also likely that interstitial fibrosis may succeed subendocardial fibrosis and appear only during subsequent phases of remodelling. If that is the case, the excess of alcian blue staining observed in the interstitium at days 7 and 28 postinfarction may presumably antedate subsequent fibrosis deposition.

Interstitial fibrosis is attributable among other factors to local renin-angiotensin system activation (Sun *et al.* 1994; Weber *et al.* 1995; de Carvalho Frimm *et al.* 1997) leading to enhanced collagen production by cardiac fibroblasts (Sun & Weber 1996). There is activation of tissue metalloproteinases (Deten *et al.* 2001), ventricular dilatation and myocardial fibrosis accumulation. As the extracellular matrix changes in the subendocardial layer seem to antedate those appearing in the interstitium, we speculate that interstitial fibrosis may result from prior subendocardial injury. By affecting the integrity of the subendocardial layer of the remote myocardium, the decrease in coronary driving pressure may indeed impair diastolic function, further augment left ventricular end-diastolic pressure and diastolic stress and thus result in left ventricular dilatation and dysfunction.

Study limitations

The pathological changes occurring in the subendocardial non-infarcted region most likely account for a reparative process to myocyte necrosis. In fact, nuclear pyknosis and karyolysis, cytoplasmic vacuolization and hypereosinophilia were usually found in that region at the acute phases. It has to be acknowledged, however, that nuclear pyknosis and cytoplasmic hypereosinophilia appear in both cell necrosis and programmed cell death processes (Saxena *et al.* 2002). The means utilized in the present study to identify myocyte cell death were exclusively morphological and thus not reliable to differentiate cell necrosis from apoptosis. Accordingly, myocyte necrosis may have been overestimated. In addition, the participation of apoptosis in subendocardial injury remains unclear.

Non-sulphated glycosaminoglycans alone were contemplated in the present study. The recognized role of proteoglycans and sulphated glycosaminoglycans in remodelling remain to be addressed taking into account subendocardial and interstitial regions of the remote non-infarcted myocardium (Endo *et al.* 1997; Doi *et al.* 2000). The latest follow-up interval examined was 28 days when glycosaminoglycans, but not collagen, appeared in greater amounts in the non-infarcted interstitial myocardium. The hypothesis that this may represent an intermediary phase in the remodelling process taking place in the interstitium needs to be addressed using longer periods of follow-up.

In the present study, the pathological changes observed in the subendocardium represent an indirect evidence of an ongoing ischaemic process affecting that region. It remains to be established whether or not low perfusion pressure actually translates into impaired myocardial blood flow to the subendocardium, in particular. As the coronary flow reserve may also be impaired after infarction (Karam *et al.* 1990; Kalkman *et al.* 1996), it remains unsettled as to what extent the decrease

in the coronary driving pressure might be counterbalanced by the vasodilating capacity of coronary resistance vessels.

Clinical implications

The present findings suggest that the use of vasodilator drugs following infarction may be potentially harmful provided myocardial perfusion is jeopardized by the reduction in systemic blood pressure. In cases of heart failure and elevated left ventricular filling pressure, the assessment of coronary driving pressure may be useful to tailor the degree to which left ventricular end-diastolic pressure may be reduced without impairing perfusion pressure.

Conclusions

Distinctive subendocardial and interstitial remodelling occurs in the remote non-infarcted myocardium. The pathological changes observed indicate that subendocardial fibrosis represents a reparative process in response to early and ongoing low perfusion pressure. The impairment in coronary driving pressure seems to be related to left ventricular dysfunction by contributing to progressive ventricular remodelling.

References

Baldwin H.S., Lloyd T.R., Solursh M. (1994) Hyaluronate degradation affects ventricular function of the early postlooped embryonic rat heart in situ. *Circ. Res.* **74**, 244–252.

Cohn J.N., Ferrari R., Sharpe N. (2000) Cardiac remodeling – concepts and clinical implications: a consensus paper from an international forum on cardiac remodeling. Behalf of an International Forum on Cardiac Remodeling. *J. Am. Coll. Cardiol.* **35**, 569–582.

Cross C., Riechen P., Salisbury P. (1961) Coronary driving pressure and vasomotor tonus as determinants of coronary blood flow. *Circ. Res.* **9**, 589–600.

de Carvalho Frimm C., Sun Y., Weber K.T. (1997) Angiotensin II receptor blockade and myocardial fibrosis of the infarcted rat heart. *J. Lab. Clin. Med.* **129**, 439–446.

de Carvalho Frimm C., Koike M.K., Cúri M. (2003) Subendocardial fibrosis in remote myocardium results from reduction of coronary driving pressure during acute infarction in rats. *Arq. Bras. Cardiol.* **80**, 515–520.

Deten A., Holz A., Leicht M., Barth W., Zimmer H.G. (2001) Changes in extracelular matrix and in transforming growth factor beta isoforms after coronary artery ligation in rats. *J. Mol. Cell. Cardiol.* **33**, 1191–1207.

Dobaczewski M., Bujak M., Zymek P., Ren G., Entman M.L., Frangogiannis N.G. (2006) Extracellular matrix remodeling in canine and mouse myocardial infarcts. *Cell Tissue Res.* **324**, 475–488.

Doi M., Kusachi S., Murakami T. *et al.* (2000) Time-dependent changes of decorin in the infarct zone after experimentally induced myocardial infarction in rats: comparison with biglycan. *Pathol. Res. Pract.* **196**, 23–33.

Endo C., Kusachi S., Ninomiya Y. *et al.* (1997) Time dependent increases in syndecan-1 and fibroglycan messenger RNA expression in the infarct zone after experimentally induced myocardial infarction in rats. *Coron. Artery Dis.* **8**, 155–161.

Kalkman E.A., Bilgin Y.M., van Haren P., van Suylen R.J., Saxena P.R., Schoemaker R.G. (1996) Determinants of coronary reserve in rats subjected to coronary artery ligation or aortic banding. *Cardiovasc. Res.* **32**, 1088–1095.

Karam R., Healy B.P., Wicker P. (1990) Coronary reserve is depressed in postmyocardial infarction reactive cardiac hypertrophy. *Circulation* **81**, 238–246.

Kumar V., Abbas A.K., Fausto N.. (2004) *Robbins and Cotran's Pathologic Basis of Disease*. Ed. Elsevier Health Sciences, Philapdelphia, PA pp 19–26.

Michel J.B., Lattion A.L., Salzmann J.L. *et al.* (1988) Hormonal and cardiac effects of converting enzyme inhibition in rat myocardial infarction. *Circ. Res.* **62**, 641–650.

Pfeffer M.A., Pfeffer J.M., Fishbein M.C. (1979) Myocardial infarct size and ventricular function in rats. *Circ. Res.* **44**, 503–512.

Pfeffer J.M., Pfeffer M.A., Braunwald E. (1985) Influence of chronic captopril therapy on the infarcted left ventricle of the heart. *Circ. Res.* **57**, 84–95.

Savani R.C., Hou G., Liu P. *et al.* (2000) A role of hyaluronan in macrophage accumulation and collagen deposition after bleomycin-induced lung injury. *Am. J. Respir. Cell Mol. Biol.* **23**, 475–484.

Saxena A., McMeekin J.D., Thomson D.J. (2002) Expression of Bcl-x, Bcl-2, Bax, and Bak in endarterectomy and atherectomy specimens. *J. Pathol.* **196**, 335–342.

Selye H., Bajuusj E., Grasso S., Mendell P. (1960) Simple techniques for the surgical occlusion of coronary vessels in the rat. *Angiology* **11**, 398–407.

Sun Y. & Weber K.T. (1996) Angiotensin converting enzyme and myofibroblasts during tissue repair in the rat heart. *J. Mol. Cell. Cardiol.* **28**, 851–858.

Sun Y., Cleutjens J.P., Diaz-Arias A.A., Weber K.T. (1994) Cardiac angiotensin converting enzyme and myocardial fibrosis in the rat. *Cardiovasc. Res.* **28**, 1423–1432.

Sun Y., Zhang J.Q., Zhang J., Lamparter S. (2000) Cardiac remodeling by fibrous tissue after infarction in rats. *J. Lab. Clin. Med.* **135**, 316–323.

Toyota E., Ogasawara Y., Hiramatsu O. *et al.* (2005) Dynamics of flow velocities in endocardial and epicardial coronary arterioles. *Am. J. Physiol. Heart Circ. Physiol.* **288**, H1598–1603.

Van Kerckhoven R., Kalkman E.A.J., Saxena P.R., Schoemaker R.G. (2000) Altered cardiac collagen and associated changes in diastolic function of infarcted rats hearts. *Cardiovasc. Res.* **46**, 316–323.

Volders P.G., Willems I.E., Cleutjens J.P., Arends J.W., Havenith M.G., Daemen M.J. (1993) Interstitial collagen is increased in the non-infarcted human myocardium after myocardial infarction. *J. Mol. Cell. Cardiol.* **25**, 1317–1323.

Waldenstrom A., Martinussen H.J., Gerdin B., Hallgren R. (1991) Accumulation of hyaluronan and tissue edema in experimental myocardial infarction. *J. Clin. Invest.* **88**, 1622–1628.

Wang J., Abraham T.P., Korinek J., Urheim S., McMahon E.M., Belohlavek M. (2005) Delayed onset of subendocardial diastolic thinning at rest identifies hypoperfused myocardium. *Circulation* **111**, 2943–2950.

Weber K.T., Pick R., Jalil J.E., Janicki J.S., Carroll E.P. (1989) Patterns of myocardial fibrosis. *J. Mol. Cell. Cardiol.* **21**(Suppl 5), 121–131.

Weber K.T., Sun Y., Katwa L.C., Cleutjens J.P., Zhou G. (1995) Connective tissue and repair in the heart. Potential regulatory mechanisms. *Ann. N. Y. Acad. Sci.* **752**, 286–299.

Wei S., Chow L.T.C., Sanderson J.E. (2000) Effect of carvedilol in comparison with metoprolol on myocardial collagen postinfarction. *J. Am. Coll. Cardiol.* **36**, 276–281.

Whittaker P., Boughner D.R., Kloner R.A. (1991) Role of collagen in acute myocardial infarct expansion. *Circulation* **84**, 2123–2134.

Wilke A., Funck R., Rupp H., Brilla C.G. (1996) Effect of the renin-angiotensin-aldosterone system on the cardiac interstitium in heart failure. *Basic Res. Cardiol.* **91**(Suppl 2), 79–84.

Yu C.M., Tipoe G.L., Wing-Hon L.K., Lau C.P. (2001) Effects of combination of angiotensin-converting enzyme inhibitor and angiotensin receptor antagonist on inflammatory cellular infiltration and myocardial interstitial fibrosis after acute myocardial infarction. *J. Am. Coll. Cardiol.* **38**, 1207–1215.